International Symposium on Hydraulic
Structures

May 16th, 10:50 AM

Three-dimensional Flow Structure Inside the Cavity of a Non-aerated Stepped Chute

Daniel Valero
FH Aachen, valero@fh-aachen.de

Jochen Vogel
FH Aachen

Daniel Schmidt
FH Aachen

Daniel B. Bung
FH Aachen, bung@fh-aachen.de

Follow this and additional works at: https://digitalcommons.usu.edu/ishs

Recommended Citation

Three-dimensional Flow Structure Inside the Cavity of a Non-Aerated Stepped Chute

D. Valero[1,2], J. Vogel[1], D. Schmidt[1] & D.B. Bung[1]

[1]*Hydraulic Engineering Section (HES), FH Aachen University of Applied Sciences, Aachen, Germany*
[2]*Dept. of ArGEnCo, Research Group of Hydraulics in Environmental and Civil Engineering (HECE), University of Liège (ULg), Liège, Belgium*
E-mail: valero@fh-aachen.de

Abstract: *Accurate energy dissipation estimation and improved knowledge on stepped spillways and stepped revetments flow structure may allow safer design of hydraulic and coastal structures. In this study, an ADV Vectrino Profiler has been used to obtain dense observations of the three-dimensional flow structure occurring inside a cavity of 20 cm to 10 cm (length to height) for four flow cases. The obtained friction factors show a strong inverse dependence on the Reynolds number. The displacement length also shows a reduction with increasing Reynolds number, which may indicate that the flow "feels" the cavity more at smaller streamwise velocities. Streamwise and normalwise velocities reveal both a turbulent boundary layer type of flow (upper flow region) and a jet impact and recirculation inside of the cavity. Spanwise median velocities allowed insight on the uncertainty levels of the ADV Vectrino Profiler measurements.*

Keywords: ADV Vectrino profiler, stepped spillways, stepped revetments, shear velocity, skin friction coefficient, friction factor.

1. Introduction

Stepped geometries are one of the simplest macro-roughness configurations that can be found in hydraulic and coastal structures. Stepped spillways have been built for thousands of years (Chanson 2002) and an increase on the community's interest has been experienced during these last decades with the use of Roller Compacted Concrete given the easiness of construction. Furthermore, the enhanced friction on the spillway allows safe conveyance of the water flow to the downstream end while yielding an earlier trigger of self-aeration when compared to classic smooth spillways. In coastal applications, stepped revetments ensure protection against wave overtopping while allowing accessibility to the structure (Kerpen and Schlurmann 2016, Kerpen et al. 2017). Despite the transient nature of the flow, energy dissipating properties of the revetment geometry are often related to the overtopping volumes.

The main characteristics of stepped spillway flows have been extensively investigated (see Chanson et al. 2015), both by means of experimental modelling (Chamani and Rajaratnam 1999, Chanson and Toombes 2002, Boes and Hager 2003, Pfister and Hager 2011, Bung 2011, Meireles et al. 2012) and numerical modelling (Bombardelli et al. 2011, Valero and Bung 2015, Lopes et al. 2017, Toro et al. 2017). Stepped spillway research can be considered a mature discipline, and its flows have been used for instrumentation and new experimental benchmarking techniques (Bung 2013, Felder and Chanson 2014, Shearin-Feimster et al. 2015, Bung and Valero 2016, Valero and Bung 2017, Felder and Pfister 2017). Nonetheless, when it comes to friction factor estimation, some concerns are still open for discussion. Recently, Felder and Chanson (2015) gathered experimental data from different studies and showed a scatter of the friction factor (f) ranging from 0.02 to 0.70, with a certain data clustering in the range of 0.1 to 0.4. Moreover, the previous dataset review of Chanson et al. (2002) showed scatter reaching f values up to 5. Thus, reducing this uncertainty becomes of paramount interest to allow safe design of future stepped energy dissipater structures. A better understanding of the flow structure may shed light on the energy dissipating mechanisms, allowing improved design of the cavity geometry. Only the previous study of Amador et al. (2006) thoroughly investigated the flow structure over a stepped cavity in the non-aerated region. Flow velocities over a stepped cavity (at least both over niches and edges) in the aerated region of stepped spillways can be found in the studies of Bung (2009), Bung (2011), Felder and Chanson (2011), Bung and Valero (2015), Bung and Valero (2016), Zhang and Chanson (2016a), and Zhang and Chanson (2018).

In this study, a stepped geometry (of 20 cm and 10 cm length and height, 2V:1H for an equivalent stepped spillway, 2H:1V for a coastal revetment) has been installed in a horizontal channel where comprehension on the flow structure is gained by means of an Acoustic Doppler Velocimetry (ADV) Vectrino Profiler (Nortek®). All studied flows correspond to subcritical flow conditions. Mean and fluctuating velocities were previously obtained by Nezu and Rodi (1986) for both subcritical and supercritical open channel flows not observing any difference. To the

knowledge of the authors of this study, only the study of Amador et al. (2006), in a 1.25V:1H setup can be compared on the level of spatial detail in the non-aerated region flow description. The main advantage of the ADV Vectrino Profiler is the access to temporally detailed velocity data with also good spatial resolution. Data is properly filtered to allow accurate estimations of streamwise velocities, normalwise velocities, shear velocities, skin friction coefficients and friction factors. Spanwise velocities, which should null for such a symmetric configuration, resulted in values commonly below 1 cm/s. Discussion between the energy dissipating properties and other flow parameters is also presented.

2. Experimental Setup

The experiments were carried out at the Hydraulics Laboratory of FH Aachen. A stepped setup was installed in a 12 m long and 0.58 m wide horizontal flume. The macro-roughness geometry was placed close to the downstream end of the flume to avoid any perturbation advection from the flume inlet. Water was recirculated from a downstream basin to a small inlet basin. The inlet basin was filled with stones, a fine polymer grid, and a 5 cm metal grid to reduce the inlet influence on the main stream. The flow rate was controlled with a frequency regulator connected to the pump and measured by means of a magnetic flow meter.
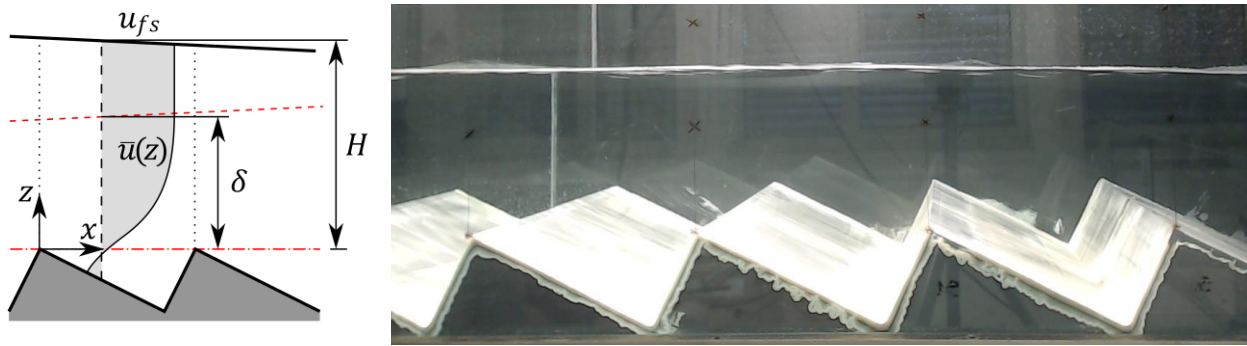

Figure 1. Left: cavity flow structure and main flow variables (free stream velocity u_{fs}, streamwise velocity expected value $\bar{u}$, flow depth H and boundary layer thickness δ). In red, pseudo-bottom and edge of the boundary layer. Right: experimental setup. Flow from left to right.

The stepped geometry was 2.70 m long and composed of 12 equal steps. The steps were intentionally sloped to simulate an equivalent stepped spillway with 2V:1H slope or a coastal protection revetment of 2H:1V, i.e.: 20 cm and 10 cm step faces (Fig. 1). The corresponding roughness height (k_v) is 8.9 cm. The herein studied model permitted observations of subcritical flows—with considerably larger flow depths than common stepped spillways laboratory models—altogether with clear water conditions. This allowed the use of ADV techniques which would fail to provide accurate results in the counterpart aerated spillway/wave runup flow. An ADV Vectrino Profiler (ADV Vectrino Profiler, Nortek®) was used to map the three-dimensional flow. The ADV Vectrino Profiler measuring range was set to 30 mm, with cells of 1 mm. The sampling rate was set to 100 Hz and the sampling time was chosen to be 300 s after a time sensitivity analysis. The ping algorithm was set to "maximum interval", as recommended by Thomas et al. (2017), and the velocity range was fixed higher than the expected velocities (above mean value plus three standard deviations). Seeding was added on demand to keep mean SNR values above 15 dB and mean correlation above 70 %, despite instantaneous values may fall below. Two different types of seeding particles were used; the first consisted of fine clay particles and the second one was the seeding particle provided by Nortek® (Table 1). For both types of particles, the seeding was performed in the channel inlet ensuring homogeneous mixing with the flow.

Four different specific discharges (q), with Reynolds numbers (R) ranging from 3.45×10⁴ to 1.21×10⁵ and subcritical Froude (F) numbers, were studied (Table 1) to allow overview of different flow conditions. The measurements were carried out following a densely spaced 20 mm by 20 mm measuring grid in both x and z directions, which resulted in some overlapping of vertical velocity profiles. Accurate probe positioning was accomplished using a bidirectional, computer controlled motor system (isel®). All velocities were measured at the sixth step cavity.

Table 1. Description of the conducted experiments.

q (m²/s)	H (m)	H/k_v (-)	F (-)	R (-)	Seeding
0.035	0.15	1.68	0.19	34,500	Nortek®
0.052	0.15	1.68	0.28	51,700	Nortek®
0.086	0.13	1.47	0.59	86,200	Fine clay
0.121	0.16	1.79	0.60	120,700	Fine clay

3. ADV Data Filtering

Velocities were measured with an ADV Vectrino Profiler (Nortek®) and the data was subsequently processed using MATLAB® in-house implemented codes as follows:

1. Velocity was temporally filtered using Goring and Nikora (2002) approach as modified by Wahl (2003).

2. Instantaneous velocity data with SNR values below 5 dB were rejected.

3. Instantaneous velocity data with correlation values below 60 % were rejected.

4. The expected value of the velocity ($\bar{u}$) was obtained by applying the median operator to the remaining temporal data series.

5. Finally, spatial filtering based on the mean velocity gradient equation is applied, following Valero and Bung (2018).
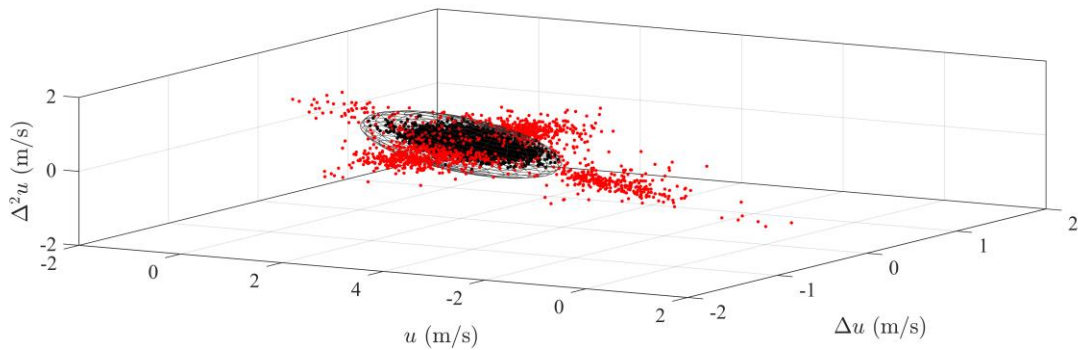

Figure 2. Ellipsoid (black mesh) resulting from application of Goring and Nikora (2002) as modified by Wahl (2003) to data gathered at q = 0.121 m²/s, x = 14 cm and z = 5 cm. Black markers for accepted data and red markers for rejected data. Percentage of total rejected data: 8.7 %.

Goring and Nikora (2002) proposed a filtering technique based on the observation that "good data" tends to cluster inside an ellipsoid defined in the coordinate system built using the velocity data and its finite differences up to second-order (u, Δu and $\Delta^2 u$, respectively). Wahl (2003) proposed some modifications to Goring and Nikora (2002), for instance, use of robust estimators to obtain the expected velocity value and variance and rejection of all the velocity components when an outlier is detected in any of the velocity components. Exemplary velocity filtering is shown in Fig. 2. Thresholds considered for SNR and correlation values were based on the study of Leng and Chanson (2015) on the unsteady estimation of turbulence in undular and breaking bores. Other studies have suggested higher thresholding values of SNR and correlation, but lower instantaneous values are not necessarily associated to erroneous data and application of Goring and Nikora (2002) and Wahl (2003) may reject a relevant part of the outliers. Thomas et al. (2017) also discussed the commonly used SNR and correlation's thresholds and its validity for the Vectrino Profiler data.

4. Results

4.1. General Remarks

Data files gathered with the ADV Vectrino Profiler were converted to MATLAB® format for postprocessing, as discussed in the previous section. The Vectrino Profiler was moved vertically up to the point where the free surface disturbed the measurement significantly (i.e., air entrainment after large free surface curvatures). Hence, the maximum velocity measured by the instrumentation may not correspond to the maximum velocity of the profile and further analysis becomes necessary.

In this study, the mean gradient equation was used to approximate the velocity gradients and extend the velocity profiles further from the measured range. The mean velocity gradient can be written as (Nikora et al. 2002, Monin and Yaglom 2007):

$$\frac{\mathrm{d}\,\bar{u}(z)}{\mathrm{d}\,z} = \frac{u_*}{\kappa(z + d_r)} \tag{1}$$

with $\bar{u}$ the expected value of the velocity (usually, the temporally averaged value), z the vertical coordinate normal to the pseudo-bottom (line connecting the edges of the steps, Fig. 1), κ the von Kármán constant, u_* the shear velocity (which represents a stress in the dimensions of velocity) and d_r the displacement length (Nikora et al. 2002). It must be noted that integration of Eq. (1) can lead to the well-known log law velocity profile. Further discussion on the validity and limitations of Eq. (1) and its parameters can be found in Valero and Bung (2018).

The shear velocity u_* and the displacement length d_r were estimated for each flow rate at the first section (over the edge) with data corresponding to $z > 0.1\,H$ and the von Kármán constant was taken as 0.40, as recommended by Monin and Yaglom (2007) or Davidson (2015). This, together with Eq. (1), allowed direct extrapolation of the velocity profiles. On the question of where velocity stops increasing and meets the free stream flow region, another condition becomes necessary. Continuity condition can be used to locate the boundary layer thickness. Therefore, the velocity profile was integrated to obtain the specific flow rate. The relation between the velocity and the specific flow rate can be written as:

$$q_{int} = \int_0^H \bar{u}(z)\,\mathrm{d}\,z = \int_0^\delta \bar{u}(z)\,\mathrm{d}\,z + (H - \delta)\,u_{fs} \tag{2}$$

being δ the boundary layer thickness and u_{fs} the free stream velocity. As the flow rate is known, q_{int} can be increased by increasing δ and adjusting the new velocities using Eq. (1) up to matching the measured specific flow rate (q). Integral of Eq. (2) was approximated by means of trapezoidal numerical integration. Obtained values of u_{fs}, δ and the ratio q_{int}/q (as an indicator related to flow continuity) are presented in Table 2 below. The ratio q_{int}/q remains below 1 for the cases where the boundary layer cannot grow farther as it intersects the free surface.

The values of u_* and d_r shown in Table 2 correspond to the data at any x coordinate and $z > 0.1\,H$ and incorporates data from all the step cavity sections, thus representing a "cavity-averaged" result. Backward finite differences were obtained and linear fitting to the inverse of Eq. (1) was used to approximate u_* and d_r (likewise Nikora et al. 2002 or Valero and Bung 2018).

It can be observed that the displacement length, which is the depth that the flow eddies "feel" (Goring et al. 2002), reduces with increasing R. The displacement length in stepped spillway flows was previously numerically studied by Cheng et al. (2014) which found that d_r/k_v was in the order of 0.22 to 0.27. Only the highest flow discharge case herein studied falls within this range. The shear velocity increases but, nonetheless, the free stream velocity increased further thus yielding a reduction of the friction factor with increasing R. Cheng et al. (2014) also noted an increase of the shear velocity with increasing discharge (i.e., with increasing R) and with increasing roughness height.

4.2. Energy Dissipation

Given that the free stream velocity and the shear velocity have been computed, the skin friction coefficient can be obtained as (Pope 2000):

$$c_f = 2\left(u_*/u_{fs}\right)^2 \tag{3}$$

The friction factor can be computed as (Pope 2000):

$$f = 8\left(\frac{u_*}{\overline{U}}\right)^2 \tag{4}$$

where the mean velocity $\overline{U}$ can be computed as q/H. Results from use of Eqs. (3) and (4) are included in Table 2. Obtained values fall above the data clustering range suggested by Felder and Chanson (2015): $0.1 \leq f \leq 0.4$ but within the scatter observed by Chanson et al. (2002). For completeness, comparison with the value obtained from the simplified theoretical model of Chanson et al. (2002) is also considered:

$$f_C = \frac{2}{K\sqrt{\pi}} \tag{5}$$

with $K \approx 6$, related to the rate of expansion of the air-water shear layer of a plunging jet (Brattberg and Chanson 1998). This yields $f_C = 0.188$. However, Chanson (2002) argued that $K \approx 12$ for monophase flows, which would result in $f_C = 0.094$, despite previously Brattberg and Chanson (1998) suggested $K \approx 11$ which would yield similarly $f_C = 0.103$.

Analogy with a shear layer flow seems clear. Nonetheless, the intensity of the shear layer or its expansion rate may depend upon other parameters as the macro-roughness geometry, described by the cavity length and cavity height (or alternatively, by the slope and the step height). With intermediate slopes, the cavity will comparatively have a larger area/volume than for very steep or mild slopes. In the limiting case of extremely flat slopes, it should be expected to converge to the smooth spillway friction value. Additionally, flow interaction with the cavity, and ultimately the energy dissipation in macro-roughness flows, can be affected by the submergence, i.e.: the ratio between flow depth (or boundary layer thickness) and the macro-roughness length scale (Cheng 2017).

The skin friction coefficients obtained in this study show a decay with increasing R, similar to d_r. Both d_r and c_f hold a Pearson correlation coefficient, as defined by Zwillinger and Kokoska (2000), of 0.9998 (however, note the small number of samples), which may imply that the lesser the flow "feels" the cavity, the smaller is the energy dissipation. At the same time, with increasing R, the flow "rolls" over the step, intruding less into the cavity. This reasoning might be useful in the design of more efficient energy dissipating surfaces in hydraulic structures, as investigated by Zhang (2017) and Zhang and Chanson (2017).

Table 2. Main characteristics of the studied cavity flow cases. Free stream velocity (u_{fs}) and boundary layer thickness (δ) estimated at the first edge of the studied cavity. Shear velocity (u_*) and displacement length (d_r) obtained with all the cavity data at $z > 0.10\,H$, skin friction coefficient (c_f) and friction factor (f).

q (m²/s)	u_* (m/s)	d_r (m)	d_r/k_v (-)	u_{fs} (m/s)	δ (m)	δ/k_v (-)	q_{int}/q (-)	c_f (-)	f (-)
0.0345	0.1014	0.091	1.01	0.3455	0.15	1.68	0.934	0.172	1.555
0.0517	0.1490	0.077	0.86	0.5354	0.15	1.68	0.976	0.155	1.495
0.0862	0.2238	0.046	0.52	0.9293	0.13	1.47	0.979	0.116	0.932
0.1207	0.2009	0.023	0.26	0.9472	0.09	1.01	1.000	0.090	0.553

4.3. Streamwise Velocity

The streamwise velocity ($\bar{u}$) is the main component of the flow under study. It contains the larger part of momentum and energy and thus, its accurate determination becomes of higher interest. In the recent studies of Brand et al. (2016), Thomas et al. (2017) and Koca et al. (2017), it was noticed that the accuracy of the ADV Vectrino Profiler is not constant for all the bins of the profile. Koca et al. (2017) recommended use of data of the Sweet-Spot (SS) $+/-8$ bins to ensure velocity estimations remained below a 10 % error. Consequently, it is often suggested to use a reduced measuring range to avoid the increasing error in the ending measuring bins. The methodology proposed by

Valero and Bung (2018) aims to detect the lowest performing streamwise velocity estimations and reject them. Thus, all the 30 bins (of 1 mm size) of the ADV Vectrino Profiler were used in this study and Valero and Bung (2018) filtering approach was used.

Figure 3 shows the streamwise velocity for all four contemplated cases. The free stream flow can only be clearly observed in Fig. 3d; all other flow cases had the boundary layer thickness closer to the free surface and out of the measuring range of the ADV Vectrino Profiler (Table 2). The minimum velocities measured inside the cavity are on average -12.5 % of the free stream velocity u_{fs}, with all four minimum velocity measurements falling between $+/-2$ % of -12.0 % of u_{fs}. Closer inspection into the data of Amador et al. (2006) shows that the minimum velocity corresponded to -15 %, -13 %, -16 % and -17 % of u_{fs}. These values are close to the herein reported but are slightly greater, which could be given by the different cavity geometry of the previous study (1.25V:1H), which may ease the flow recirculation. Also, data scatter in Amador et al. (2006) is similar to the scatter herein reported.
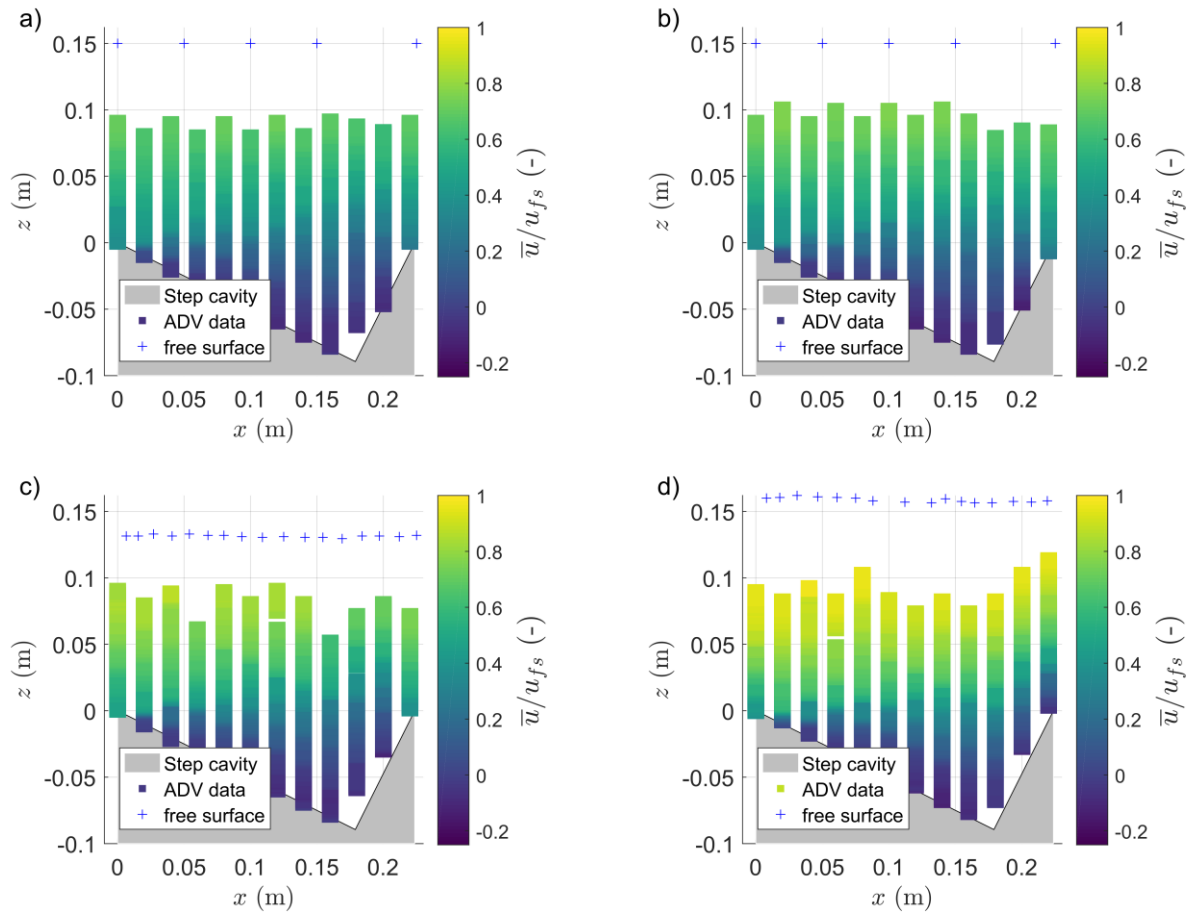

Figure 3. Streamwise velocity for a) $q = 0.035$ m²/s, b) $q = 0.052$ m²/s, c) $q = 0.086$ m²/s, d) $q = 0.121$ m²/s.

4.4. Spanwise Velocity

Mean velocity transverse to the stream flow direction ($\bar{v}$) can be expected to vanish given the two-dimensional nature of the flow. However, some ADV misalignment could take place yielding small transverse components. Moreover, Zedel and Hay (2011) found that ADV Profiler often yields non-null lateral velocities which, moreover, do not overlap. A measure of the misalignment can be obtained through the angle θ:

$$\theta(z) = \text{atan}\left(\frac{\bar{v}(z)}{\bar{u}(z)}\right) \tag{6}$$

The median misalignment θ obtained using the data of all the bins for each of the studied flow rates is (from smaller flow rate to higher flow rate): $-0.19º$, $-0.31º$, $1.3º$ and $0.70º$, which indicates a proper positioning of the Vectrino Profiler for all the analysed flow conditions. When using only the data from the SS, these angles generally were 2 to 20 % smaller in magnitude. This misalignment has been corrected for all the flow velocity distributions and, consequently, the streamwise velocity component shown in Fig 3 already incorporated the small transverse velocity contribution.

Nonetheless, some additional transverse mean flux is still estimated by the Vectrino Profiler, which should be acknowledged as erroneous (Zedel and Hay 2011). Using data of all 30 bins, the median of the absolute deviation of $\bar{v}$ for all four considered flow cases always remained below 1 cm/s. This magnitude can be understood as a measure of the random transverse velocity artificially introduced by the Vectrino Profiler, as discussed by Zedel and Hay (2011). Hence, compared to the expected velocities shown in Table 2, it is rather a relative small source of error.

It must be noted that transverse velocity fluctuations are non-zero, as it can be expected for any boundary layer type of flow (Jiménez and Hoyas 2008, Pope 2000).

4.5. Normalwise Velocity

Flows with gradients in the flow depth or the channel bed can present non-null vertical velocities (Castro-Orgaz and Hager 2017 pp. 102). In the case under consideration, the cavity produces a clockwise recirculation (Fig. 3), which must be necessarily accompanied of significant vertical velocities. Data shown in Fig. 4 corresponds to the median normalwise velocity ($\bar{w}$). This velocity component cannot be filtered with the mean velocity gradient method proposed by Valero and Bung (2018). However, a simple median filter with the same window size suggested by Valero and Bung (2018) is used.
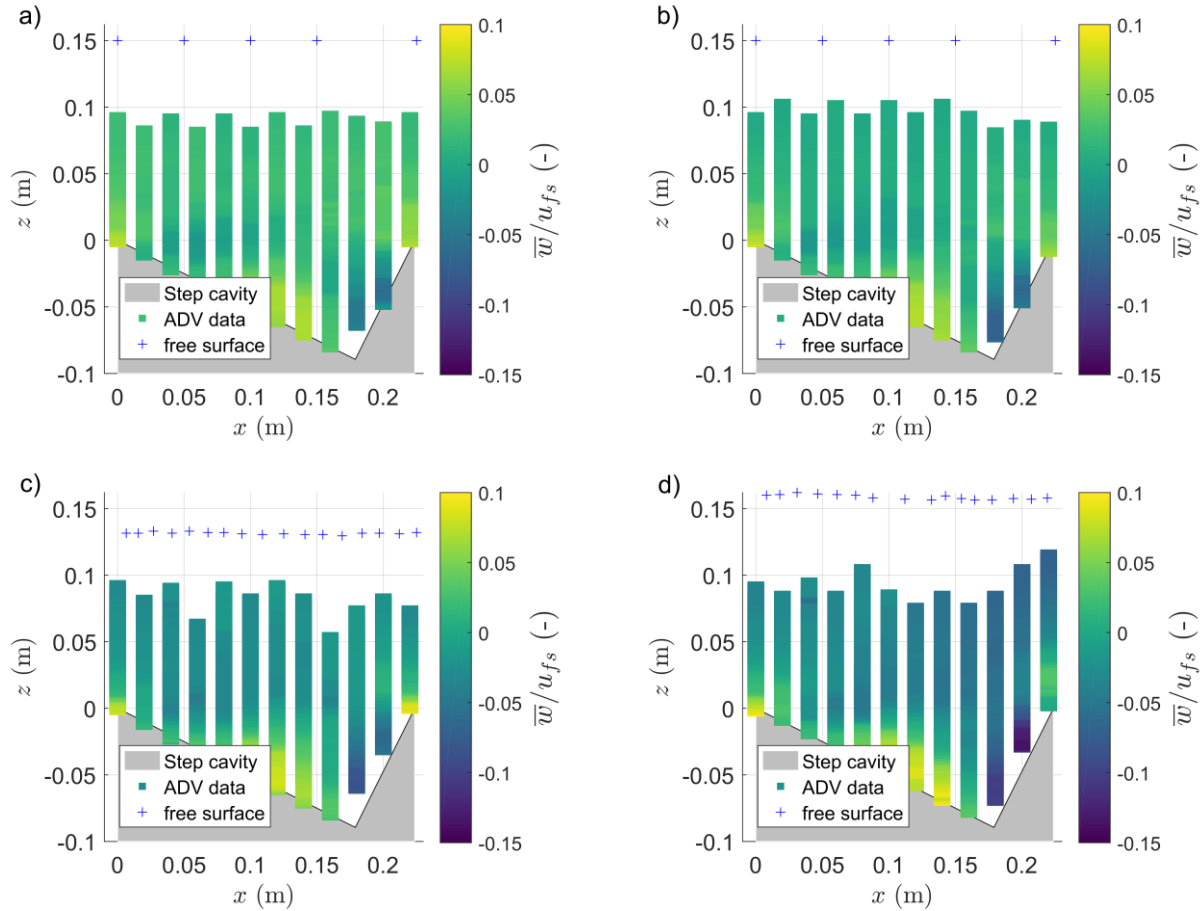

Figure 4. Normalwise velocity for a) $q = 0.035$ m²/s, b) $q = 0.052$ m²/s, c) $q = 0.086$ m²/s, d) $q = 0.121$ m²/s.

Minimum and maximum normalwise velocities take place inside the cavity and occur close to the wall, as a jet type flow after the streamwise flow impacts on the opposing cavity face. Use of the data of a large number of bins around the SS is of interest to access the velocities closer to the wall. However, the farther from the SS, the lower the quality (Thomas et al. 2017, Koca et al. 2017, Brand et al. 2016, MacVicar et al. 2014). Moving median is not applied (differently to Fig. 4) to this data to avoid smoothing of the extreme values. However, the choice of these values is made based upon the histogram of $\bar{w}$—with data from SS $+/-$ 8 bins, as recommended by Koca et al. (2017) for velocity estimations—with 100 histogram bins, which allow visual detection of outliers. This estimation may depend upon the number of histogram bins but is more robust than direct (and blind) estimation of the minimum or maximum value of $\bar{w}$. Values obtained for the minimum $\bar{w}$ correspond to -11.3 % of u_{fs} and maximum values group around 9.8 % of u_{fs}. It seems reasonable that the magnitude of the minimum value is larger than that of the maximum values given that the minimum values are closer to the jet impact on the cavity and follow a more inclined plane (thus the vertical projection is larger). After the impact of the jet against the cavity face, flow acceleration can be observed which might be accompanied by a local rise of the pressure (previously observed by Amador et al 2009 and Zhang and Chanson 2016b). Jet velocity decay can be also observed inside the cavity (Figs. 3 and 4), which can be typically found in turbulent jets (Rajaratnam 1976), while vertical velocity acceleration is found close to the step edge, where maximum flow shearing occurs.

5. Conclusions

Literature on the estimation of friction factors on stepped spillways shows a considerably large scatter (Chanson et al. 2002, Felder and Chanson 2015) when compared to literature on macro-roughness (Cheng 2017). Furthermore, there are still many unresolved issues related to the key parameters affecting the energy dissipation (Hunt et al. 2017). Accurate friction factor estimation and better knowledge on stepped spillways and stepped revetments flow structure may allow safer design of hydraulic and coastal structures.

In this study, a stepped geometry has been setup in a 12 m long and 0.58 m wide horizontal channel at the Hydraulics Laboratory of the FH Aachen. An ADV Vectrino Profiler has been used to obtain dense observations of the three-dimensional flow structure occurring inside a cavity of 20 cm to 10 cm (length to height) for four flow cases, with F ranging between 0.19 to 0.60, R between 3.45×10^4 to 1.21×10^5 and k_v/H around 0.57. Velocity time series were filtered using Goring and Nikora (2002) method as modified by Wahl (2003). Low SNR and correlation velocity estimations were also removed and spatial filtering based on Valero and Bung (2018) was applied to filter physically inconsistent velocity estimations.

The obtained skin friction factors show a strong (inverse) dependence on the Reynolds number. The displacement length also shows a reduction with increasing Reynolds number, which may indicate that the flow "feels" the cavity more at smaller streamwise velocities. Streamwise and normalwise velocities reveal the interaction between both a turbulent boundary layer type of flow (main flow region) and a jet impact and recirculation region inside of the cavity. Obtained values of the friction factor fall above the clustering values obtained by Felder and Chanson (2015) but within the scatter of Chanson et al. (2002). Spanwise median velocities allowed insight on the uncertainty levels of the ADV Vectrino Profiler measurements.

6. Acknowledgements

7. References

Amador, A., Sánchez-Juny, M., and Dolz, J. (2006). "Characterization of the nonaerated flow region in a stepped spillway by PIV." *Journal of Fluids Engineering*, *128*(6), 1266-1273. doi: 10.1115/1.2354529.

Amador, A., Sánchez-Juny, M., and Dolz, J. (2009). "Developing flow region and pressure fluctuations on steeply sloping stepped spillways." *Journal of Hydraulic Engineering*, 135(12), 1092-1100. doi: 10.1061/(ASCE)HY.1943-7900.0000118.

Boes, R. M., and Hager, W. H. (2003). "Two-phase flow characteristics of stepped spillways." *Journal of Hydraulic Engineering*, 129(9), 661-670. doi: 10.1061/(ASCE)0733-9429(2003)129:9(661).

Bombardelli, F. A., Meireles, I., and Matos, J. (2011). "Laboratory measurements and multi-block numerical simulations of the mean flow and turbulence in the non-aerated skimming flow region of steep stepped spillways." *Environmental Fluid Mechanics*, 11(3), 263-288. doi: 10.1007/s10652-010-9188-6.

Brand, A., Noss, C., Dinkel, C., and Holzner, M. (2016). "High-resolution measurements of turbulent flow close to the sediment–water interface using a bistatic acoustic profiler." *Journal of Atmospheric and Oceanic Technology*, 33(4), 769-788.

Brattberg, T., and Chanson, H. (1998). "Air Entrapment and Air Bubble Dispersion at Two-Dimensional Plunging Water Jets." Chemical Engineering Science, 53(24), 4113-4127. Errata: 1999, 54(12), 1925. doi: 10.1016/S0009-2509(98)80004-3.

Bung, D. B. (2009). *Zur selbstbelüfteten Gerinneströmung auf Kaskaden mit gemäßigter Neigung*. PhD thesis (in German), Bergische Universität Wuppertal, Germany.

Bung, D. B. (2011). "Developing flow in skimming flow regime on embankment stepped spillways." *Journal of Hydraulic Research*, *49*(5), 639-648. doi: 10.1080/00221686.2011.584372.

Bung, D. B. (2013). "Non-intrusive detection of air–water surface roughness in self-aerated chute flows." *Journal of Hydraulic Research*, 51(3), 322-329. doi: 10.1080/00221686.2013.777373.

Bung, D. B., and Valero, D. (2015). "Image processing for Bubble Image Velocimetry in self-aerated flows". Proc., *36th IAHR World Congress,* 28 June – 3 July, 2015, The Hague, the Netherlands.

Bung, D. B., and Valero, D. (2016). "Optical flow estimation in aerated flows." *Journal of Hydraulic Research*, 54(5), 575-580. doi: 10.1080/00221686.2016.1173600.

Castro-Orgaz, O., and Hager, W. H. (2017). *Non-Hydrostatic Free Surface Flows*. Springer, Advances in geophysical and Environmental Mechanics and Mathematics. doi: 10.1007/978-3-319-47971-2.

Chamani, M. R., & Rajaratnam, N. (1999). "Characteristics of skimming flow over stepped spillways." *Journal of Hydraulic Engineering*, *125*(4), 361-368. doi: 10.1061/(ASCE)0733-9429(1999)125:4(361).

Chanson, H. (2002). *The Hydraulics of Stepped Chutes and Spillways*. Balkema Publishers. ISBN: 9058093522.

Chanson, H., Yasuda, Y., and Ohtsu, I. (2002). "Flow resistance in skimming flows in stepped spillways and its modelling." *Canadian Journal of Civil Engineering*, 29(6), 809-819. doi: 10.1139/l02-083.

Chanson, H.; Bung, D.B. and Matos, J. (2015): "Stepped spillways and cascades." In: Chanson, H. (Ed.): *Energy Dissipation in Hydraulic Structures* (IAHR monograph), CRC Press, ISBN 978-1-13-802755-8.

Chanson, H., and Toombes, L. (2002). "Air–water flows down stepped chutes: turbulence and flow structure observations." *International Journal of Multiphase Flow*, *28*(11), 1737-1761. doi: 10.1016/S0301-9322(02)00089-7.

Cheng, N. S. (2017). "Simple Modification of Manning-Strickler Formula for Large-Scale Roughness." *Journal of Hydraulic Engineering*, *143*(9), 04017031. doi: 10.1061/(ASCE)HY.1943-7900.0001345.

Cheng, X., Gulliver, J. S., & Zhu, D. (2014). "Application of displacement height and surface roughness length to determination boundary layer development length over stepped spillway." *Water*, 6(12), 3888-3912. doi: 10.3390/w6123888.

Davidson, P. A. (2015). *Turbulence. An Introduction for Scientists and Engineers*. Second Edition. Oxford University Press.

Felder, S., and Chanson, H. (2011). "Air-water flow properties in step cavity down a stepped chute." *International Journal of Multiphase Flow*, 37(7), 732-745. doi: 10.1016/j.ijmultiphaseflow.2011.02.009.

Felder, S., and Chanson, H. (2014). "Triple decomposition technique in air–water flows: application to instationary flows on a stepped spillway." *International Journal of Multiphase Flow*, *58*, 139-153. doi: 10.1016/j.ijmultiphaseflow.2013.09.006.

Felder, S., and Chanson, H. (2015). "Simple design criterion for residual energy on embankment dam stepped spillways." *Journal of Hydraulic Engineering*, *142*(4), 04015062. doi: 10.1061/(ASCE)HY.1943-7900.0001107.

Felder, S., and Pfister, M. (2017). "Comparative analyses of phase-detective intrusive probes in high-velocity air–water flows." *International Journal of Multiphase Flow*, 90, 88-101. doi: 10.1016/j.ijmultiphaseflow.2016.12.009.

Goring, D. G., and Nikora, V. I. (2002). "Despiking acoustic Doppler velocimeter data." *Journal of Hydraulic Engineering*, 128(1), 117-126. doi: 10.1061/(ASCE)0733-9429(2002)128:1(117).

Hunt, S. L., Kadavy, K. C., and Crookston, B. M. (2017). Discussion of "Simple Design Criterion for Residual Energy on Embankment Dam Stepped Spillways" by Stefan Felder and Hubert Chanson. *Journal of Hydraulic Engineering*, *143*(5), 07017001. doi: 10.1061/(ASCE)HY.1943-7900.0001283.

Jiménez, J., and Hoyas, S. (2008). "Turbulent fluctuations above the buffer layer of wall-bounded flows." *Journal of Fluid Mechanics*, *611*, 215-236.

Kerpen, N., and Schlurmann, T. (2016). "Stepped revetments–Revisited." Proc.: *6th International Conference on the Application of Physical Modelling in Coastal and Port Engineering and Science (Coastlab16)*.

Kerpen, N. B., Bung, D. B., Valero, D., and Schlurmann, T. (2017). "Energy dissipation within the wave run-up at stepped revetments." *Journal of Ocean University of China*, 16(4), 649-654. doi: 10.1007/s11802-017-3355-z.

Koca, K., Noss, C., Anlanger, C., Brand, A. and Lorke, A. (2017). "Performance of the Vectrino Profiler at the sediment–water interface." *Journal of Hydraulic Research*, 573-581. doi: 10.1080/00221686.2016.1275049.

Leng, X., and Chanson, H. (2015). "Unsteady turbulence during the upstream propagation of undular and breaking tidal bores: an experimental investigation." *University of Queensland Report No. CH98/15*.

Lopes, P., Leandro, J., Carvalho, R. F., and Bung, D. B. (2017). "Alternating skimming flow over a stepped spillway." *Environmental Fluid Mechanics*, 17(2), 303-322. doi: 10.1007/s10652-016-9484-x.

MacVicar, B.J., Dilling, S., Lacey, R.W.J., and Hipel, K. (2014). "A quality analysis of the Vectrino II instrument using a new open-source MATLAB toolbox and 2D ARMA models to detect and replace spikes." Proc., *River Flow 2014* (Editors: A. J. Schleiss, G. De Cesare, M. J. Franca, M., and Pfister, M.). CRC Press, Taylor & Francis.

Meireles, I., Renna, F., Matos, J., & Bombardelli, F. (2012). "Skimming, nonaerated flow on stepped spillways over roller compacted concrete dams." *Journal of Hydraulic Engineering*, *138*(10), 870-877. doi: 10.1061/(ASCE)HY.1943-7900.0000591.

Nezu, I., & Rodi, W. (1986). "Open-channel flow measurements with a laser Doppler anemometer." *Journal of Hydraulic Engineering*, 112(5), 335-355. doi: 10.1061/(ASCE)0733-9429(1986)112:5(335).

Nikora, V., Koll, K., McLean, S., Dittrich, A., and Aberle, J. (2002). "Zero-plane displacement for rough-bed open-channel flows." Proc., *River Flow 2002 - Proceedings of the International Conference on Fluvial Hydraulics, (Editors: D. Bousmar & Y. Zech)*.

Pfister, M., and Hager, W. H. (2011). "Self-entrainment of air on stepped spillways." *International Journal of Multiphase Flow*, *37*(2), 99-107. doi: 10.1016/j.ijmultiphaseflow.2010.10.007.

Pope, S. B. (2000). *Turbulent Flows*. Cambridge University Press.

Rajaratnam, N. (1976). *Turbulent Jets*. Elsevier, Developments in Water Sciences, 5.

Shearin-Feimster, L. E., Crookston, B. M., and Felder, S. (2015). "Design approaches and numerical modelling of a stepped spillway under high tailwater conditions." Proc., *35th Annual USSD Conf.*, United States Society on Dams, Denver, USA.

Thomas, R. E., Schindfessel, L., McLelland, S. J., Creëlle, S., and De Mulder, T. (2017). "Bias in mean velocities and noise in variances and covariances measured using a multistatic acoustic profiler: the Nortek Vectrino Profiler." *Measurement Science and Technology* 28(7), 075302.

Toro, J. P., Bombardelli, F. A., and Paik, J. (2017). "Detached Eddy Simulation of the Nonaerated Skimming Flow over a Stepped Spillway." *Journal of Hydraulic Engineering*, 143(9), 04017032. doi: 10.1061/(ASCE)HY.1943-7900.0001322.

Valero, D., and Bung, D. B. (2015). "Hybrid investigations of air transport processes in moderately sloped stepped spillway flows." Proc., e-*proceedings of the 36th IAHR World Congress*, The Hague, Netherlands.

Valero, D., and Bung, D. B. (2017). "Artificial Neural Networks and pattern recognition for air-water flow velocity estimation using a single-tip optical fibre probe." *Journal of Hydro-environment Research*. doi: 10.1016/j.jher.2017.08.004.

Valero, D., and Bung, D. B. (2018). "Vectrino Profiler spatial filtering for shear flows based on the mean velocity gradient equation." *Journal of Hydraulic Engineering*. doi: 10.1061/(ASCE)HY.1943-7900.0001485.

Wahl, T. L. (2003). Discussion of "Despiking acoustic doppler velocimeter data" by Goring D. G. and Nikora V. I. (2002). *Journal of Hydraulic Engineering*, 129(6), 484-487. doi: 10.1061/(ASCE)0733-9429(2003)129:6(484).

Zedel, L., and Hay, A. E. (2011). "Turbulence measurements in a jet: comparing the Vectrino and Vectrino II." Proc., *IEEE/OES/CWTM 10th Working Conference on Current Measurement Technology*.

Zhang, G., and Chanson, H. (2016a). "Interaction between free-surface aeration and total pressure on a stepped chute." *Experimental Thermal and Fluid Science*, 74, 368-381. doi: 10.1016/j.expthermflusci.2015.12.011.

Zhang, G., and Chanson, H. (2016b). "Hydraulics of the developing flow region of stepped spillways. II: Pressure and velocity fields." *Journal of Hydraulic Engineering*, 142(7), 04016016. doi: 10.1061/(ASCE)HY.1943-7900.0001136.

Zhang, G. (2017). *Free-Surface Aeration, Turbulence, and Energy Dissipation on Stepped Chutes with Triangular Steps, Chamfered Steps, and Partially Blocked Step Cavities*. PhD Thesis, The University of Queensland, Australia.

Zhang, G., and Chanson, H. (2017). "Air-Water Flow Properties in Stepped Chutes with Modified Step and Cavity Geometries." *International Journal of Multiphase Flow*. doi: 10.1016/j.ijmultiphaseflow.2017.11.009.

Zwillinger, D., and Kokoska, S. (2000). *Standard Probability and Statistical Tables and Formulae*. Chapman & Hall, CRC Press. ISBN: 1-58488-059-7.

Zhang, G., and Chanson, H. (2018). "Application of local optical flow methods to high-velocity free-surface flows: Validation and application to stepped chutes." *Experimental Thermal and Fluid Science*, 90, 186-199. doi: 10.1016/j.expthermflusci.2017.09.010.